university of groningen

University Medical Center Groningen

University of Groningen

Nanocavity formation processes in MgO(100) by light ion (D, He, Li) and heavy ion (Kr, Cu, Au) implantation

Veen, A. van; Fedorov, A.V.; Schut, H.; Labohm, F.; Kooi, Bart; De Hosson, J.T.M.

Published in:
Nuclear Instruments & Methods in Physics Research Section B-Beam Interactions with Materials and Atoms

DOI:
10.1016/S0168-583X(02)00620-1

IMPORTANT NOTE: You are advised to consult the publisher's version (publisher's PDF) if you wish to cite from it. Please check the document version below.

Document Version
Publisher's PDF, also known as Version of record

Publication date:
2002

Link to publication in University of Groningen/UMCG research database

Citation for published version (APA):
Veen, A. V., Fedorov, A. V., Schut, H., Labohm, F., Kooi, B. J., & Hosson, J. T. M. D. (2002). Nanocavity formation processes in MgO(100) by light ion (D, He, Li) and heavy ion (Kr, Cu, Au) implantation. Nuclear Instruments & Methods in Physics Research Section B-Beam Interactions with Materials and Atoms, 191(1), 610 - 615. [PII S0168-583X(02)00620-1]. DOI: 10.1016/S0168-583X(02)00620-1

Copyright
Other than for strictly personal use, it is not permitted to download or to forward/distribute the text or part of it without the consent of the author(s) and/or copyright holder(s), unless the work is under an open content license (like Creative Commons).

Take-down policy
If you believe that this document breaches copyright please contact us providing details, and we will remove access to the work immediately and investigate your claim.

Downloaded from the University of Groningen/UMCG research database (Pure): http://www.rug.nl/research/portal. For technical reasons the number of authors shown on this cover page is limited to 10 maximum.

Download date: 10-02-2018

ELSEVIER

Nuclear Instruments and Methods in Physics Research B 191 (2002) 610–615

NIM B
Beam Interactions with Materials & Atoms

www.elsevier.com/locate/nimb

Nanocavity formation processes in MgO(1 0 0) by light ion (D, He, Li) and heavy ion (Kr, Cu, Au) implantation

A. van Veen [a,*], M.A. van Huis [a], A.V. Fedorov [a], H. Schut [a], F. Labohm [a], B.J. Kooi [b], J.Th.M. De Hosson [b]

[a] *Interfaculty Reactor Institute, Delft University of Technology, Mekelweg 15, NL-2629 JB Delft, The Netherlands*
[b] *Department of Applied Physics, Materials Science Centre, University of Groningen, Nijenborgh 4, NL-4797 AG Groningen, The Netherlands*

Abstract

In studies on the controlled growth of metallic precipitates in MgO it is attempted to use nanometer size cavities as precursors for formation of metallic precipitates. In MgO nanocavities can easily be generated by light gas ion bombardment at room temperature with typically 30 keV ion energy to a dose of 10^{16} cm^{-2}, followed by annealing to 1300 K. It has been shown earlier by transmission electron microscopy (TEM) that the cavities (thickness 2–3 nm and length/width 5–10 nm) have a perfectly rectangular shape bounded by {1 0 0} faces. The majority of the gas has been released at this temperature and the cavities are stable until annealing at 1500 K. The depth location of the cavities and the implanted ions is monitored by positron beam analysis, neutron depth profiling, RBS/channeling and energy dispersive spectroscopy. The presence of metallic nanoprecipitates is detected by optical absorption measurements and by high-resolution XTEM. Surprisingly, all the metallic implants induce, in addition to metallic precipitates in a band at the mean ion range, small rectangular and cubic nanocavities. These are most clearly observed at a depth shallower than the precipitate band. In the case of gold the cavities are produced in close proximity to the crystal surface. The results indicate that in MgO vacancy clustering dominates over Frenkel-pair recombination. Results of molecular dynamics calculations will be used to discuss the observed defect recovery and clustering processes in MgO. © 2002 Elsevier Science B.V. All rights reserved.

1. Introduction

Metallic nanoprecipitates embedded in insulating materials show optical effects of importance for the development of new materials for opto-electronics and integrated optics [1], and for electronic and magnetic applications. Control of the precipitate formation process is very limited. Depth of the precipitates can be chosen by the implantation energy, but precipitate size, density and uniformity depend in a strongly correlated way on the ion fluence, the implantation temperature and the annealing temperature. The precipitate shape is governed by laws of thermal equilibrium. Recently, results have been reported of studies where precipitate formation has been tried in two steps. First, cavities are formed by light ion bombardment followed by annealing [2,3]. In a second step, the metal was introduced by bombardment with metal ions followed by

* Corresponding author. Tel.: +31-15-2782801; fax: +31-15-2786422.
E-mail address: avveen@iri.tudelft.nl (A. van Veen).

0168-583X/02/$ - see front matter © 2002 Elsevier Science B.V. All rights reserved.
PII: S0168-583X(02)00620-1

annealing to diffuse the metal atoms to the pre-existing cavities [4,5]. The formation of cavities proceeds easily and leads in MgO to perfectly rectangular or cubic shaped cavities with faces parallel to {1 0 0} MgO crystal planes [6]. Though it has been observed that the metal atoms are trapped by the cavities, conditions not yet have been optimal to collect all the metal atoms in the cavities. One of the drawbacks is trapping and agglomeration of the metal atoms at implantation defects. To our surprise, heavy ion implantation leads to considerable additional cavity formation adjacent to the implantation zone. In this paper the formation process of nanocavities during light and heavy ion bombardment is studied.

2. Sample treatment and analysis methods

Commercially available polished MgO(1 0 0) samples are used. Implantation was performed in implanters at the universities of Delft (30 and 280 keV), Groningen (50 keV) and Alabama (600 keV and 1 MeV). Doses and other implantation conditions are given in Table 1. Usually the samples were implanted at RT, with the exception of the 30 keV Au implanted sample. In all other cases the samples were annealed isothermally at temperature ranging from RT to $T > 1473$ K. Annealing took place in ambient air for the duration of 1 h. After the annealing steps the depth profile of defects was monitored by positron beam analysis (PBA) and photon absorption measurements. In PBA the shape of the Doppler broadened 511 keV photon peak resulting from annihilation of positrons in the sample is monitored while the implantation depth of the positrons is varied. In MgO the average implantation depth of the positrons varies from 0 to 1.5 μm when the positron energy varies from 0 to 30 keV. Open volume defects, e.g. vacancies, vacancy clusters and voids are identified by a relative increase of annihilations with low momentum electrons which is expressed by the parameter S [7].

In the case of 50 keV Cu and 1 MeV Au RBS was applied to measure the depth distribution of the implanted metal atoms. Energy dispersive spectroscopy (EDS) on cross-sectional transmission electron microscopy (TEM) samples was used to measure Au and Kr depth distributions. In a number of cases cross-sectional TEM was performed at the final annealing temperature. Neutron depth profiling (NDP) was applied to measure the depth profile of the implanted ^{3}He

Table 1
MgO(1 0 0) ion implanted samples; implantation data and defect observations

Implantation				TRIM results					Nanocavities			Ref.
Ion	E_{ion} (keV)	Dose (1E16 cm^{-2})	T_{impl} (K)	R_p (ΔR_p)/ nm	Displ. (vac/ion)	Conc. (MgO fraction)	Damage displacement per MgO (dpa)		T_{anneal} (K)	Location of cavity zones (nm)		
							Surface	Maximum near R_p		PBA	XTEM	
D	15	2	RT	150 (34)	6	0.050	0.01	0.04	950	130	100	[2]
^{3}He	30	1	RT	160 (41)	23	0.019	0.02	0.09	1350	100–110	100–140	[3]
Cu	50	1	RT	26 (8)	250	0.076	3.7	5.6	1350	0–15 70–110	5–15	[8]
Kr	280	3	RT	102 (27)	1000	0.073	11.2	22.4	1075	15–40 180–300	15–30	
Au	30	3	1273	14 (3)	170	0.841	11.2	16.8	–	[a]	10	[5]
Au	30	1	RT	14 (3)	170	0.281	3.7	5.6	1373	[a]	10	[5]
Au	1000	1	RT	160 (31)	3300	0.022	5.6	18.7	1273	25–175 280–450		[4]
									1473	[b]	–	

[a] Depth too small for PBA observation.
[b] Voids dissolved at this temperature.

and ^{6}Li during annealing. In Table 1 an overview is given of the implantation conditions for a selection of the samples that were studied.

3. Results and discussion

3.1. Positron beam analysis and electron microscopy

Positron beam analysis shows that for all implantations vacancy type defects are created by the implantation. However, depending on their concentration the vacancies disappear after annealing or form nanocavities. An example of the evolution of the vacancy profile is given in Fig. 1 for a 1 MeV Au ion implanted sample. In the as-implanted sample a modest increase of S is observed mainly in a region at smaller depth than the implantation depth of the gold. We ascribe this to trapping and annihilation in vacancies or small vacancy clusters. After annealing to 773 K a considerable increase of S is observed in the wide depth range from 20 to 500 nm indicating that vacancy clustering has occurred. From 773 to 1273 K a development is seen of a depth distribution consisting of two peaks. The valley between the two peaks is located at the position of the implanted Au. This sample was annealed to 1473 K before a cross-sectional TEM observation was done. At 1473 K nearly all cavities in MgO dissolve so that only a band of gold precipitates was observed. The above double peaked vacancy cluster or void distribution is typical for implantation of heavy ions and has been observed for Au, Ag, Cu and Kr implantation. See Table 1 for the cavity zones identified by PBA. It must be remarked that the affinity of positrons for open volume defects is that high that already at levels of 0.1% vacancies saturation trapping occurs. In this case we expect saturation trapping in the first peak at shallow depth already after implantation. The second peak at large depth might be due to considerably lower vacancy concentrations and therefore to non-saturated trapping.

Bands of cavities are only observed in XTEM samples when heavy ions are used with sufficiently high dose. Examples are given in Figs. 2(a) and (b) for respectively Au implanted [4] at 1273 K and for Cu post-implantation annealed to 1350 K [8]. Also

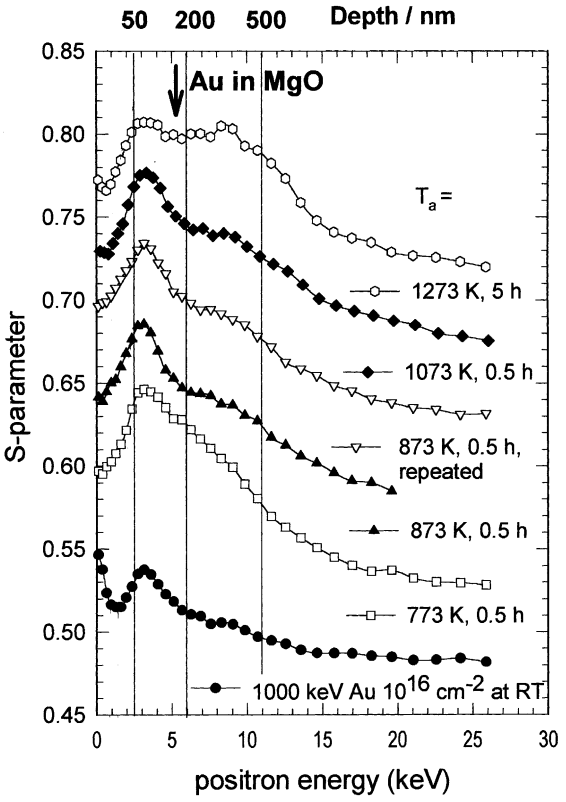

Fig. 1. The positron annihilation S-parameter plotted as function of the positron implantation energy for a 1 MeV gold ion implanted MgO(1 0 0) crystal. Curves are shown for the as implanted sample and after annealing to the indicated temperatures. To separate the curves the curves are shifted each time vertically with a value ($S = 0.05$). Note the depth scale indicated on the top of the figure. The arrow indicates the implantation depth of the gold atoms.

for Kr and Au implanted at RT and annealed to high temperatures cavity bands are observed (see Table 1). The band of cavities is situated between the surface and the implantation layer where nanoprecipitates are formed by the implanted atoms. TEM does not give firm evidence for cavities beyond the implantation depth of the heavy ions. It might be that the density and size of the voids is too low for TEM observation but sufficient for considerable trapping of positrons.

No cavities are observed for the light ions D, He and Li. However, in the case of D and He gas bubbles are formed in the implantation zone, which eventually convert into nanocavities when

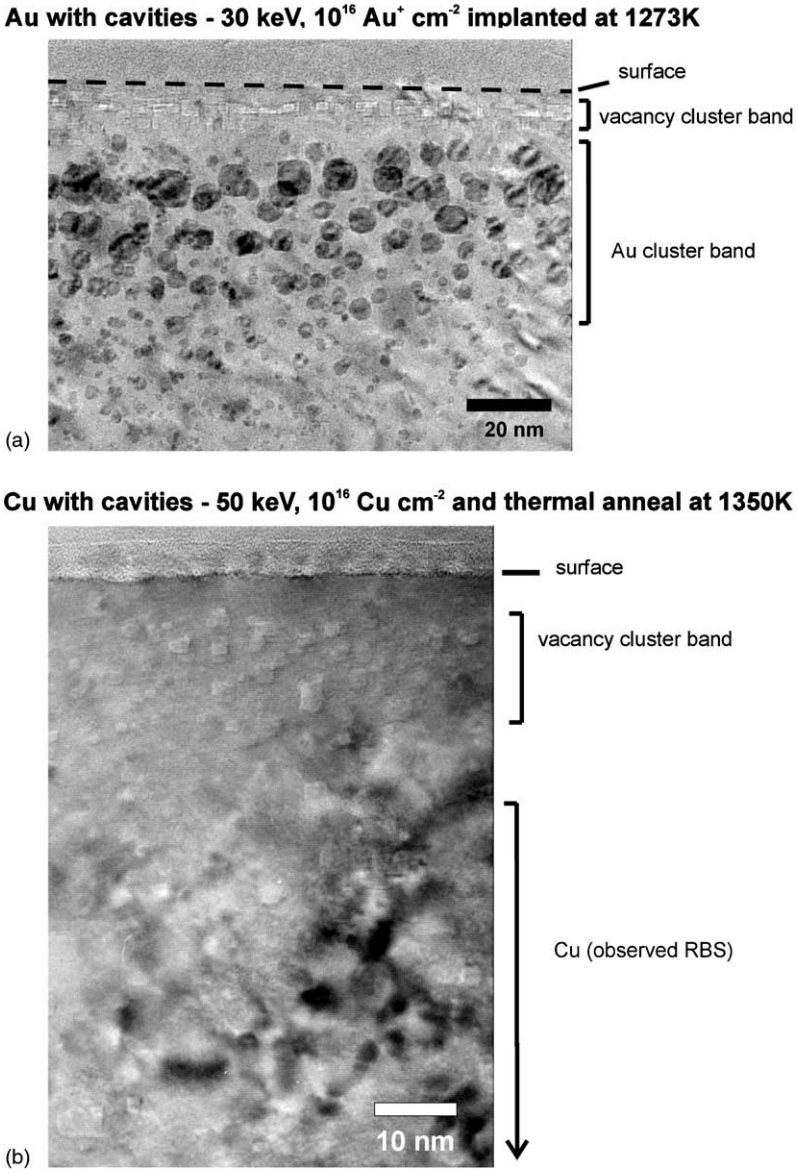

Fig. 2. Cross-sectional TEM micrographs obtained for (a) gold ion and (b) copper ion implanted MgO(1 0 0). See Table 1 for details.

the gas is released from the bubbles: for D and He this transition from bubbles to nanocavities takes place at 950 and 1300 K respectively [2,3]. Lithium forms metallic Li precipitates without a cavity zone. At temperatures of 1450 K nanocavities disappear. Therefore, no cavities are observed in the Au implanted sample which was annealed to 1473 K.

3.2. Nucleation and growth of cavities

From the results it emerges rather clearly that vacancy clusters and nanocavities nucleate and grow rather easily in MgO. At room temperature the vacancies are not mobile but interstitials are [10]. At an annealing temperature of about 550 K vacancies become mobile and trigger the vacancy

clustering process. Optical absorption measurements indicate that F centers (oxygen vacancies with a trapped electron) disappear at this temperature. The fact that a certain fraction of the vacancies survives recombination with interstitials must be ascribed to the formation of interstitial dislocation loops which form a bias for trapping of interstitials. Kooi et al. [6] show that in helium implanted MgO dislocation loops with $1/2\,a\langle 1\,1\,0\rangle$ Burgers vector are formed on $\{1\,1\,0\}$ crystallographic planes. Similar loops are reported by Clinard et al. for neutron irradiated MgO [10]. Agglomeration of vacancies is preferred in a 3D fashion. Busker et al. [9] calculated that a cubic cluster containing four Schottky pairs (V_{Mg}–V_O) is energetically favourable over a planar defect with the same amount of Schottky pairs. It is likely that during annealing Ostwald ripening occurs with the extremely stable cavities bounded by (1 0 0) surfaces remaining in the final stage. The difference in surface energy between the (1 0 0) and the other low index surfaces amounts at least a factor of 2 so that cavities formed by these surfaces are stable to much higher temperatures than cavities with other faces, even to temperatures where self-diffusion is fast. If metals are present the internal cavity surfaces get covered by metal atoms and these cavities might shrink easily until they are filled completely by a metal cluster. The driving force is the energy gain by wetting the MgO surfaces with a metal. Thus cavities will only develop in areas where the metal to dpa ratio is small. In Fig. 3 (top) the depth dependent displaced atom concentration (dpa) and the Au concentration is given for 30 keV Au implantation. Low ratios are found for depth <10 and >20 nm. At the same time the dpa level is high near the surface. At large depth dpa levels are two orders of magnitude lower. Qualitatively similar concentrations are calculated for 50 keV Cu, 280 keV Kr and 1000 keV Au. The XTEM results for Cu and Au prove that vacancy clusters develop in the zone with low metallic implant to dpa ratio. PBA appears to be able also to detect the second, deeper lying, zone where cavities are developing. The reason why dpa concentration extends deeper than the implants is due to recoils generated by the heavy ion implants. This effect is completely absent when light ion implantation is

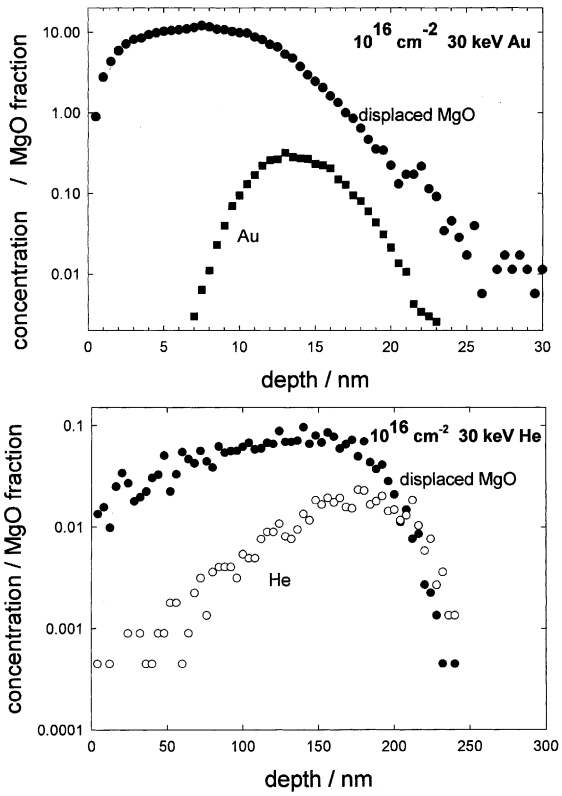

Fig. 3. Concentration profiles of displaced atoms Mg–O and implanted atoms Au and He calculated by the TRIM code for 30 keV Au (top) and 30 keV He (bottom) implanted in MgO to a dose of 10^{16} cm^{-2}.

considered. In the bottom of Fig. 3 it is observed that dpa levels for helium implantation are small and that in the end of range damage the He to dpa ratio exceeds unity. Thus there is no opportunity to create vacancies in the tail of the implantation.

It is of interest to note that in light ion irradiation nanocavities are formed at the implantation depth of the light ions by forming bubbles first. Later during thermal annealing helium or deuterium permeates from the bubble zone to the surface leaving behind nanocavities at the implantation depth.

4. Conclusions

Nanocavities in heavy ion implanted MgO have been identified by PBA and cross-sectional TEM.

It has been concluded that (1 0 0) bounded nanocavities form easily when vacancy concentrations are high (remaining after displacement levels >100 dpa). Stabilisation of 3D vacancy clusters by gas atoms is not a requirement for cavity growth in MgO. Low concentrations of cavities in the tail of the implantation are well detected by PBA.

References

[1] C.W. White, J.D. Budai, S.P. Withrow, J.G. Zhu, E. Sonder, R.A. Zuhr, A. Meldrum, D.M. Hembree Jr., D.O. Henderson, S. Prawer, Nucl. Instr. and Meth. B 141 (1998) 228.

[2] A. van Veen, H. Schut, A.V. Fedorov, E.A.C. Neeft, R.J.M. Konings, B.J. Kooi, J.Th.M. de Hosson, Nucl. Instr. and Meth. B 147 (1999) 216.

[3] H. Schut, A. van Veen, F. Labohm, A.V. Fedorov, E.A.C. Neeft, R.J.M. Konings, Nucl. Instr. and Meth. B 147 (1999) 212.

[4] A.V. Fedorov, A. van Veen, M.A. van Huis, H. Schut, B.J. Kooi, J.Th. De Hosson, R.L. Zimmerman, Proceedings, CAARI 2000, Denton.

[5] A.V. Fedorov, M.A. van Huis, A. van Veen, H. Schut, Nucl. Instr. and Meth. B 166–167 (2000) 215.

[6] B.J. Kooi, A. van Veen, J.Th.M. de Hosson, H. Schut, A.V. Fedorov, F. Labohm, Appl. Phys. Lett. 76 (9) (2000) 1110.

[7] A. van Veen, H. Schut, P.E. Mijnarends, in: P.G. Coleman (Ed.), Positron Beams and their Applications, World Scientific, Singapore, 2000, Chapter 6, p. 191.

[8] M.A. van Huis, A.V. Fedorov, A. van Veen, P.J.M. Smulders, B.J. Kooi, J.Th.M. de Hosson, Nucl. Instr. and Meth. B 166–167 (2000) 225.

[9] G. Busker, M.A. van Huis, R.W. Grimes, A. van Veen, Nucl. Instr. and Meth. B 171 (2000) 528.

[10] F.W. Clinard Jr., G.F. Hurley, L.W. Hobbs, J. Nucl. Mater. 108–109 (1982) 655.